IAC-17-C1.9.5

VERIFICATION OF PLANETARY PROTECTION REQUIREMENTS WITH SYMPLECTIC METHODS AND MONTE CARLO LINE SAMPLING

Matteo Romano[1], Camilla Colombo[1], Jose Manuel Sánchez Pérez[2]

[1] Politecnico di Milano, Dep. of Aerospace Science and Technology, Milano, Italy, matteo1.romano@polimi.it, camilla.colombo@polimi.it
[2] ESA, European Space Operations Centre (ESOC), Darmstadt, Germany, Jose.Manuel.Sanchez.Perez@esa.int

Verification of the compliance to planetary protection requirements is an important task of interplanetary mission design, aiming to reduce the risk of biological contamination of scientifically interesting celestial bodies. This kind of analysis requires efficient and reliable numerical tools to propagate uncertainties over times up to 100 years with high precision. This paper presents a plan to improve the techniques used for planetary protection analysis in the SNAPPshot numerical tool developed at the University of Southampton for an ESA study. The Line Sampling method is presented as an alternative Monte Carlo approach to sample more efficiently the initial uncertainties, reducing the computational effort to estimate the probability of impact between uncontrolled objects and a celestial body. Symplectic integration methods are introduced as a strategy to obtain a more accurate propagation of the spacecraft trajectory starting from the initial conditions, thanks to their formulation that includes the conservation of total energy. Preliminary results are included to show the advantages and the current limitations of the proposed approaches.

I. INTRODUCTION

I.I. Planetary protection

At the injection from Earth of an interplanetary mission, the upper stage of the launcher that inserted the spacecraft into the transfer orbit also leaves the Earth's sphere of influence. These artificial bodies then follow their trajectories without the possibility to be observed or controlled, with the chance of impacting other planets or moons. These events represent a risk for scientific research, as many celestial bodies in our Solar System are highly valued targets for biological studies, presenting environmental conditions that may support microbial life. An impact from a non-sterilized man-made object could lead to contamination with Earth-based microorganisms, thus making worthless any data that could be collected in the search for extra-terrestrial life.

To protect other planets and moons from risks of contamination, each interplanetary mission must be compliant to planetary protection requirements, which set a maximum acceptable limit to the impact probability between debris from space missions with any celestial body [1]. These requirements do not only affect launchers, but also spacecraft at the end of their missions, or after they have become uncontrollable following a failure of a core subsystem.

Planetary protection accounts for such random events, alongside the uncertainty over the initial orbital state of the launcher or spacecraft (due to measurements errors during observation, or to misfiring of the propulsion system during the initial manoeuvres). These uncertainties evolve over time, making difficult to predict the actual position of the launcher or debris over periods up to 100 years, and whether an impact with a sensitive target will occur or not [2][3]. For these reasons, planetary protection requirements must be verified during the design of the space mission, affecting the final results of the mission analysis phases. Past work at the University of Southampton has developed the SNAPPshot for verification of planetary protection analysis of ESA missions [4][5][6]. The software written in modern Fortran propagates a set of initial condition deriving from a distribution function for a given amount of time through a Monte Carlo approach and computes the probability of impact with target planets with a given level of confidence. The initial distribution can represent a failure in the propulsion system, a distribution in are-to-mass of the satellite, or the covariance matrix representative of the launcher injection error.

Planetary protection verification requires precise, reliable and efficient numerical instruments and efficient techniques for uncertainty propagation. This paper presents

a strategy for improving the accuracy and the accuracy and the efficiency of the planetary protection analysis, acting in two different directions: one side is represented by the numerical integration, in order to understand how the errors in a single propagation affect the overall verification of the planetary protection requirements; on the other side, there is the sampling of the uncertainties, in order to analyse more efficient methods to sample the initial dispersion.

I.II. Proposed approach

The starting point for this research is the SNAPPshot tool suite for the verification of the compliance to planetary protection requirements developed at the University of Southampton in the framework of a study for the European Space Agency (ESA) [4][5][6]. The tool follows a Monte Carlo approach, where the initial uncertainty (over the state or other design parameters of the spacecraft or launcher) is sampled into many initial conditions, that are then propagated in order to estimate the probability of impact (or orbital resonance) with other celestial bodies. The propagations are carried out with the use of high-order Runge-Kutta methods, with different possible ways to adapt the time-step. Other functionalities are available for post-processing the trajectories, but are not treated in this work.

This paper proposes a different approach to improve numerical propagation and probability sampling in planetary protection analysis. An improved accuracy of the numerical solution and a qualitative behaviour closer to the actual evolution of the dynamic system can be obtained by introducing symplectic integration methods [7]. These, which include conservation of prime integrals in their definition, and additional energy-preserving schemes, in order to counteract the accumulation of numerical error in long-term propagations that may make the representation of the spacecraft state unreliable, especially with strongly non-linear dynamics. Impact probability is instead estimated with the use of Line Sampling [8], by solving a lower number of one-dimensional integrals along a reference direction pointing toward the impact region of the uncertainty domain; this reduces the overall computational cost of standard Monte Carlo Simulation methods, which require a very high number of input samples to obtain robust estimation of impact probability.

These two approaches to planetary protection analysis will be explained, and applied to different cases to show their performance in terms of accuracy and computational cost. In the current development, these two parts are still

addressed separately. Some study cases are chosen among the ones already considered in [4], to perform a comparison with some reference results.

The paper is organised as follows: Section II is devoted to the explanation of the Line Sampling method, accompanied by some examples showing the advantages and limitations with respect to a standard Monte Carlo approach; Section III contains a review of the integration methods that were considered in this paper, tested in a reference propagation to show how symplectic methods work; Section IV presents the application of the numerical methods previously introduced to interplanetary missions that require an analysis of their compliance to planetary protection requirements; finally, Section V will summarise the main results and present some of the objectives for continuing this work in the future.

II. SAMPLING TECHNIQUES

II.I. Line Sampling

The Line Sampling (LS) method was originally developed as a MC approach for the reliability analysis of complex structural systems with small failure probabilities [9]. It has been adapted for planetary protection analysis, and can be applied in general to the estimation of impact probability of small objects (asteroids or space debris) with major celestial bodies (regarding this topic, a comparison between the LS and Subset Simulation methods was made in [10]). The main feature of this method is the analytical estimation of the probability, obtained by reducing the multi-dimensional integration problem across the uncertainty domain to many one-dimensional problems along lines following a reference direction; this direction is determined so that it points toward the impact region of the domain, and, if this is properly chosen, the method can considerably reduce the number of required system simulations with respect to a standard MC.

The LS method follows four steps: 1) the determination of the reference direction; 2) the mapping of random samples from the physical coordinate space into a normalised standard space; 3) the probing of the impact region along the lines following the reference direction α; 4) the estimation of the impact probability. A summary of each step will be given to give a general overview of the LS technique, along with an introduction to the choices that were made in its numerical implementation.

Determination of the reference direction
There are different options to determine the reference direction [9]. For this work, it was chosen to determine it

as a normalised "centre of mass" of the impact subdomain. This region was approximated by applying the Metropolis-Hastings algorithm to generate a Markov Chain lying entirely in the impact domain (Markov Chain Monte Carlo simulation is a method for generating samples conditional on a region satisfying a given condition, according to any given probability distribution), starting from an initial condition in the impact subdomain [9]. In the current implementation, this starting condition is found with an optimisation process aimed to minimise the minimum distance from the target body. The $\boldsymbol{\alpha}$ direction is then computed in the standard normal space, as

$$\boldsymbol{\alpha} = \frac{1}{N_s} \sum_{u=1}^{N_s} \frac{\boldsymbol{\theta}^u}{\left\| \boldsymbol{\theta}^u \right\|} \qquad (1)$$

Where $\boldsymbol{\theta}^u$, $u = 1, ..., N_s$ represent the points of the Markov's chain made of N_S samples converted into the standard normal space. The choice of performing a Markov's chain of course implies the need to perform additional simulations increasing the computational effort required by the method, but this ensures that a good coverage of the impact region is obtained.

Mapping onto the standard normal space

Once a reference direction is determined, a new set of N_T random samples is generated, then mapped into the standard normal space. This transformation is a significant step, especially for problems with high-dimensionality, as each component θ_j, $j = 1, ..., n$ of the new parameter vector $\boldsymbol{\theta} \in \mathbb{R}^n$, to which $\mathbf{x} \in \mathbb{R}^n$ is mapped, is associated with a standard normal distribution. The joint Probability Density Function (PDF) of those random parameters is, then

$$\Phi(\theta) = \prod_{j=1}^{n} \phi_j(\theta_j) \qquad (2)$$

where ϕ_j indicates the PDF associated with the j-th component of $\boldsymbol{\theta}$:

$$\phi_j(\theta_j) = \frac{1}{\sqrt{2\pi}} \exp(-\frac{\theta_j^2}{2}), \quad j = 1, 2, ..., n \qquad (3)$$

This allow a simplification of the computation of the impact probability later in the procedure, as it reduces the problem to a series of one-dimensional computations, that can be carried out analytically. The direct and the inverse transformations, from the physical domain to the standardised one and vice versa respectively, preserve the Cumulative Distribution Function (CDF) between the two coordinate spaces, and are defined as:

$$\Phi(\boldsymbol{\theta}^k) = F(\mathbf{x}^k), \quad k = 1, 2, ..., N_T \qquad (4)$$

$$\boldsymbol{\theta}^k = \Phi^{-1}[F(\mathbf{x}^k)] \qquad (5)$$

$$\mathbf{x}^k = F^{-1}[\Phi(\boldsymbol{\theta}^k)] \qquad (6)$$

with Φ and F being the CDF of, respectively, the unit Gaussian distribution and the input uncertainty distribution of the problem. For this work, Rosenblatt's transformation was applied [11]; in the case of a Gaussian distribution in the uncertainty parameters (as in the cases under study, see Section 0), both the direct and the inverse transformations (respectively equations (5) and (6) become linear [9][11].

Line Sampling

Once the reference direction is defined, for every random sample $\boldsymbol{\theta}^k$, $k = 1, ..., N_T$ a line parallel to $\boldsymbol{\alpha}$ is defined in the standard normal space according to the parameter c^k, such that

$$\boldsymbol{\theta}^k = c^k \boldsymbol{\alpha} + \boldsymbol{\theta}_\perp^k \qquad (7)$$

$$\boldsymbol{\theta}_\perp^k = \boldsymbol{\theta}^k - \left\langle \boldsymbol{\theta}^k, \boldsymbol{\alpha} \right\rangle \boldsymbol{\alpha} \qquad (8)$$

This reformulates the problem as a series of one-dimensional problems associated with each sample, by exploiting the property that c^k is also normally distributed in the standard space. The standard domain is then explored along each line following the $\boldsymbol{\alpha}$ direction by evaluating a performance function for different values of c^k, in order to identify the intersections between the line and the impact subdomain, with the corresponding values of c^k. The minimum distance from the planet of interest during the propagation is chosen as a performance function in this work. Due to the nature of the problem under analysis, two intersections with the impact region are found when considering a single close approach in a given event window, with two limit values $(\overline{c}_1^k, \overline{c}_2^k)$. For this reason, and also due to the non-linear nature of the performance function, an iterative process (i.e. numerical Newton iterations) was used to identify both values, thus requiring more than one value of c^k to be evaluated for each case, with a subsequent reduction of the efficiency of this method.

Estimation of the impact probability

Once all $(\overline{c}_1^k, \overline{c}_2^k)$ are known, a conditional impact probability given by the unit Gaussian CDF is associated to each random initial condition as

$$\hat{P}^k(I) = \hat{P}[\overline{c}_1^k < N(0,1) < \overline{c}_2^k] = \Phi(\overline{c}_2^k) - \Phi(\overline{c}_1^k)$$
$$k = 1, 2, ..., N_T \qquad (9)$$

The total impact probability and variance are then approximated by

$$\hat{P}(I) = \frac{1}{N_T} \sum_{k=1}^{N_T} \hat{P}^k(I) \qquad (10)$$

$$\hat{\sigma}^2(\hat{P}(I)) = \frac{1}{N_T(N_T-1)} \sum_{k=1}^{N_T} (\hat{P}^k(I) - \hat{P}(I))^2 \qquad (11)$$

III. NUMERICAL INTEGRATION

III.I. Equations and constants of motion

The integrations of the equations of motion are carried out using Cartesian coordinates in the J2000 reference frame centred in the solar system barycentre. Non-dimensional variables are used, obtained by dividing, respectively, distance and time by

$$\bar{L} = AU, \quad \bar{t} = 2\pi\sqrt{AU^3/\mu_{Sun}} \qquad (12)$$

where μ_{Sun} is the gravitational constant of the Sun. The trajectory is propagated under the effect of gravitational forces of the Sun and all the planetary systems considered with their barycentre, except for the Earth and the Moon, considered as separate bodies. No additional perturbations such as solar radiation pressure and relativistic effects were included. Cartesian coordinates allow a Hamiltonian formulation of the problem (see paragraph III.II).

In the restricted N-body problem (RNBP), the overall gravitational acceleration is obtained from:

$$\ddot{\mathbf{r}} = -\sum_{j=0}^{N} \mu_j \frac{\mathbf{r} - \mathbf{r}_j(t)}{\left\| \mathbf{r} - \mathbf{r}_j(t) \right\|^3} \qquad (13)$$

where r_j represents the position vector of the j-th planet in barycentric coordinates (with $j=0$ indicating the Sun or, in general, the main attractor). Using Cartesian coordinates, a Hamiltonian formulation of the problem is possible, and the Hamiltonian function can be seen as the total energy of the two-body problem perturbed by the gravitational effects due to the N planets:

$$H(\mathbf{r}, \mathbf{v}, t) = \frac{1}{2} \left\| \mathbf{v} \right\|^2 - \sum_{j=0}^{N} \frac{\mu_j}{\left\| \mathbf{r} - \mathbf{r}_j(t) \right\|^3} \qquad (14)$$

It must be said that the Hamiltonian is not a true constant of the dynamics, as it depends on time explicitly (that is, it is non-autonomous) so that $d\,H/dt = \partial H/\partial t \neq 0$. To obtain a true first integral of motion, the problem is reformulated in such a way the Hamiltonian does not explicitly depend on time: a new independent variable s is introduced to write the time t as

an additional state coordinate $t = \tau(s)$ with its own conjugate momentum $u(s)$ [12]. The new Hamiltonian is thus written as

$$K(\mathbf{r}, \mathbf{v}, \tau, u) = H(\mathbf{r}, \mathbf{v}, t) + u \qquad (15)$$

The new Hamiltonian is not time-dependent anymore; the equations describing the state of the system maintain the same form:

$$\frac{d\mathbf{r}}{ds} = \frac{\partial K}{\partial \mathbf{v}} = \mathbf{v}$$

$$\frac{d\mathbf{v}}{ds} = -\frac{\partial K}{\partial \mathbf{r}} = -\sum_{j=0}^{N} \mu_j \frac{\mathbf{r} - \mathbf{r}_j(s)}{\left\| \mathbf{r} - \mathbf{r}_j(s) \right\|^3} \qquad (16)$$

while two new equations are added:

$$\frac{d\tau}{ds} = \frac{\partial K}{\partial u} = 1$$

$$\frac{du}{ds} = -\frac{\partial K}{\partial \tau} = -\frac{\partial H}{\partial t} = -\dot{H} \qquad (17)$$

Eq. (17) do not affect the numerical integration, as the state of the system is independent from them, resulting in

$$\tau(s) = s = t$$

$$u(s) = -K(s) = -H(t) \qquad (18)$$

This operation has two main advantages: first, a true constant of motion is defined, resulting that $K(\mathbf{r}, \mathbf{v}, \tau, u) = H(\mathbf{r}, \mathbf{v}, t) - H(t) = 0$; second, the Hamiltonian form of the problem is recovered.

III.II. Symplectic methods

The evolution of an autonomous (time-independent) Hamiltonian system with n degrees of freedom can be described by the Hamiltonian function $H(\mathbf{q}, \mathbf{p})$, where coordinates $\mathbf{q}$ and their conjugate momenta $\mathbf{p}$ are a set of canonical variables, thought the equations

$$q_j = \frac{\partial H}{\partial p_j}, \quad p_j = -\frac{\partial H}{\partial q_j}, \quad j = 1,...,n \qquad (19)$$

From these, the flow Φ_t^H can be defined over the domain Ω in the phase space such that $(\mathbf{q}, \mathbf{p}) = \Phi_t^H(\mathbf{q}_0, \mathbf{p}_0)$. The flow Φ_t^H is a symplectic transformation if it preserves the differential two-form $\omega = \mathbf{dp} \wedge \mathbf{dq}$ over Ω, meaning that the sum of the oriented two-dimensional volumes over the phase space is conserved in time. Many properties of Hamiltonian systems derive from the symplectic nature of the dynamic flow [13]. One of these properties is the

conservation of autonomous Hamiltonian functions in time, that is $H(\mathbf{q},\mathbf{p}) = H(\mathbf{q}_0,\mathbf{p}_0)$.

A one-step numerical integrator is in general non-symplectic, as its map Ψ_h^H in the phase space only approximates the real flow of the dynamics while advancing from one time step t_n to the next $t_{n+1} = t_n + h$ as $(\mathbf{q}_{n+1},\mathbf{p}_{n+1}) = \Psi_h^H(\mathbf{q}_n,\mathbf{p}_n)$. However, this approximation can be symplectic if it maintains the canonical structure of the dynamics between successive iterations, and differs from the exact one up to an order r: $\Psi_h^H = \Phi_h^H + O(h^{r+1})$. In this case, the numerical method is said of *r-th* order, and preserves the value of the Hamiltonian function within that accuracy.

In the following subsections, a general explanation of the methods that were selected for this work is presented. Table 1 reports a selection of integration methods that have been compared in different cases of orbital propagation. As the considered symplectic methods are all defined in a fixed-step formulation, the 8th order fixed-step RK scheme is used as a reference. The chosen methods are also tested with a regularisation of the time step according to the dynamics, following the approach already implemented in SNAPPshot (see Debatin et al. 1986 in [4]); in this case, the propagation is performed also using the adaptive step RK8(7) method [14].

Explicit and implicit Runge-Kutta methods

One-step RK schemes with s stages can become symplectic when applied to Hamiltonian dynamics if the coefficients of the Butcher's tableau $(\mathbf{A},\mathbf{b},\mathbf{c})$ satisfy the symmetric relation [15]:

$$m_{ij} = b_i a_{ij} + b_j a_{ji} - b_i b_j = 0 \quad \forall i,j = 1,...,s \tag{20}$$

In this way, the value of the Hamiltonian function will remain bounded during the integration, instead of presenting fictitious energy dissipation. However, the relation in Eq. (20) implies that explicit schemes cannot be symplectic without having all b coefficients equal to zero.

A class of symplectic implicit RK methods is represented by collocation methods. In particular, those derived from Gauss-Legendre quadrature coefficients (indicated as GLRK in Table 1) were selected for this work. These schemes are particularly efficient for orbital propagation, since they are A-stable at all orders, thus allowing larger time steps with lower error, and GLRK methods using s stages yield a solution of order *p=2s* [16]. However, implicit methods require the resolution at every step of a system of non-linear implicit equations, which can be done with the use of Newton or fixed-point iterations

[16], with the consequence that the accuracy of this iterative process will affect also the accuracy of the propagation. The first option was chosen in the implementation of the method for this work.

Runge-Kutta-Nyström methods

RKN schemes are Partitioned RK methods, which are formulated to be applied to problems presenting a separable Hamiltonian function in the form [17]

$$H(\mathbf{r},\mathbf{v}) = T(\mathbf{v}) + V(\mathbf{r}), \quad T(\mathbf{v}) = \frac{1}{2}\mathbf{v}^T\mathbf{v} \tag{21}$$

where the potential contribution V is function of the coordinate variables $\mathbf{r}$ (Cartesian position vector) only and the kinetic contribution T is function of the associated momenta $\mathbf{v}$ (Cartesian velocity vector) only, with the equations of motion taking the form

$$\dot{\mathbf{r}} = \mathbf{v}$$
$$\dot{\mathbf{v}} = \mathbf{r} = -\frac{\partial V}{\partial \mathbf{r}} = f(\mathbf{r}) \tag{22}$$

This kind of methods use two different sets of coefficients to integrate separately the coordinates and the momenta. For the integration step of length h $(\mathbf{r}_n(t_n),\mathbf{v}_n(t_n)) \rightarrow (\mathbf{r}_{n+1}(t_{n+1}),\mathbf{v}_{n+1}(t_{n+1}))$:

$$\mathbf{r}_{n+1} = \mathbf{r}_n + h\mathbf{v}_n + h^2\sum_{i=1}^{s} b_i f(t_n + c_i h, \mathbf{X}_i)$$
$$\mathbf{v}_{n+1} = \mathbf{v}_n + h\sum_{i=1}^{s} d_i f(t_n + c_i h, \mathbf{X}_i) \tag{23}$$
$$\mathbf{X}_i = \mathbf{r}_n + c_i h\mathbf{v}_n + h^2\sum_{j=1}^{s} a_{ij} f(t_n + c_j h, \mathbf{X}_j)$$
$$i = 1,...,s$$

with a Butcher's tableau $(\mathbf{A},\mathbf{b},\mathbf{d},\mathbf{c})$, where $\mathbf{b}$ are the coefficients used for the coordinates, and $\mathbf{d}$ the coefficients for the momenta.

In the case of RKN methods, also explicit schemes can be symplectic, and embedded adaptive schemes are possible [18]. To be symplectic, an *s*-stage explicit scheme with Butcher's tableau $(\mathbf{A},\mathbf{b},\mathbf{d},\mathbf{c})$ must satisfy the relations [17]

$$b_i = d_i(1-c_i), \quad i = 1,...,s$$
$$d_i(b_j - a_{ij}) = d_j(b_i - a_{ji}), \quad i,j = 1,...,s \tag{24}$$

Methods derived from Hamiltonian formulation

Some numerical integration methods can be obtained directly from the Hamiltonian formulation of the problem, through subsequent canonical transformations. The methods so derived are symplectic, meaning that the

truncation error in the total energy has no secular component, thus conserving the total energy exactly up to a certain order of accuracy [19]. These are, however, fixed-step methods, and any kind of variation of the step size during the integration generally breaks down the conservation properties.

In this work, the Yoshida integrator presented in [20] in the separable Hamiltonian was considered (SY in Table 1). Given the initial state $\mathbf{x}_0 = (\mathbf{r}_0, \mathbf{v}_0)$ at time t_0, the n-th order solution at time t_0+h is given as a product of elementary symplectic mappings of lower order:

$$\mathbf{x}(h) = \left[\prod_{i=1}^{k} \exp(c_i h D_T) \exp(d_i h D_V) \right] \mathbf{x}_0 \qquad (25)$$

where D_T and D_V are differential operators associated with the kinetic and potential terms of the Hamiltonian. The map in Eq. (25) gives a succession of k explicit mappings:

$$\mathbf{r}_{i+1} = \mathbf{r}_i + c_i h \frac{\partial \mathrm{T}}{\partial \mathbf{v}}(\mathbf{v}_i)$$

$$\mathbf{v}_{i+1} = \mathbf{v}_i - d_i h \frac{\partial \mathrm{V}}{\partial \mathbf{r}}(\mathbf{r}_{i+1}) \qquad (26)$$

$$i = 1, ..., k$$

with $\mathbf{x}_k = (\mathbf{r}_k, \mathbf{v}_k)$ being the solution at time step t_0+h.

III.III. Other numerical techniques

Step regularisation

As for the integrators already implemented in SNAPPshot [4], in this work a possible way to control the step size was implemented following Debatin's approach [21], which rescales the step according to the Jacobian matrix of the equations of motion, approximated through its maximum eigenvalue. However, one should consider that symplectic methods with a fixed-step formulation suffer from any variation of the time step for a symplectic method, losing their conservation properties and showing drift in the first integrals of motion.

Projection methods

Projection methods are numerical techniques that correct the solution obtained with other integrators to minimize the integration error on a given first integral of the dynamics (e.g. the total energy of the system). In this way, a solution closer to the physical behaviour of the system is obtained [7].

Given an arbitrary one-step method Φ_h such that $\mathbf{x}_{n+1} = \Phi_h(\mathbf{x}_n)$, where $\mathbf{x}$ represents the state vector, and given a quantity $\mathrm{I}(\mathbf{x})$ that conserves during the propagation, generally the solution given by the method do not satisfies the relation $\mathrm{I}(\mathbf{x}_{n+1}) = \mathrm{I}(\mathbf{x}_n)$. A new solution $\tilde{\mathbf{x}}_{n+1}$ such that $\mathrm{I}(\tilde{\mathbf{x}}_{n+1}) = \mathrm{I}(\mathbf{x}_n)$ can be obtained by solving a constrained minimisation problem considering the Lagrange function

$$\mathrm{L}(\tilde{\mathbf{x}}_{n+1}, \lambda) = \frac{1}{2} \left\| \tilde{\mathbf{x}}_{n+1} - \mathbf{x}_{n+1} \right\| - g(\tilde{\mathbf{x}}_{n+1})^T \lambda \qquad (27)$$

with $g(\mathbf{x}) = \mathrm{I}(\mathbf{x}) = \mathrm{I}(\mathbf{x}_0)$ being the constraint vector function, and λ a vector of Lagrange multipliers. This leads to a simplified expression

$$\tilde{\mathbf{x}}_{n+1} = \mathbf{x}_{n+1} + \nabla_y \, g(\mathbf{x}_{n+1})^T \lambda$$

$$g(\mathbf{x}_{n+1}) = 0$$

$$(28)$$

The second relation is a non-linear system of algebraic equations with λ unknown, which can be easily solved via Newton iterations:

$$\Delta \lambda_i = -\left(g'(\mathbf{x}_{n+1}) g'(\mathbf{x}_{n+1})^T \right)^{-1} g\left(\mathbf{x}_{n+1} + g'(\mathbf{x}_{n+1})^T \lambda_i \right)$$

$$\lambda_{i+1} = \lambda_i + \Delta \lambda_i \qquad (29)$$

Fly-by detection

Symplectic methods can achieve conservation of the total energy (as value of the Hamiltonian function) over long integration times. This is true in those cases when the dynamics is regular and non-chaotic during the propagation. However, close approaches with planets, especially very close fly-bys, represent conditions when the non-linearity of the dynamics drastically increases the numerical error on the solution, visible as a steep growth of position and velocity errors from the reference values, and of the total energy from the initial value. This generally affects any numerical fixed- or variable-step method.

This kind of problem has been addressed before by many authors, who devised different approaches to overcome or bypass the numerical effects of the fly-bys, by applying *ad hoc* numerical techniques only during a close approach (e.g. switching the primary body of the propagation from the main attractor to the approaching planet [22], or applying the projection technique in order to impose the conservation of energy).

Any solution, however, requires a correct identification of the close approach or fly-by conditions to counteract the increase of numerical errors in an effective way, following criteria that should be evaluated automatically during the integration. Again, different are the possible solution to accomplish this task (e.g. setting a limit distance from the approaching planet). In this work, another approach is

proposed, which considers the behaviour of the dynamics as criterion to define a close approach.

Given the equations of motion, the Jacobian matrix is defined as

$$\mathbf{J} = \frac{d\mathbf{f}}{d\mathbf{x}} = \begin{bmatrix} \mathbf{0} & \mathbf{I} \\ \mathbf{G} & \mathbf{0} \end{bmatrix} \qquad (30)$$

where $\mathbf{x}$ is the state vector, containing position and velocity vectors $\mathbf{r}$ and $\mathbf{v}$), $\mathbf{I}$ is the identity matrix and $\mathbf{G}$ results from the derivation of the gravitational terms defined in equation (13):

$$\mathbf{G} = \frac{\partial \ddot{\mathbf{r}}}{\partial \mathbf{r}} = \begin{bmatrix} \cdots & \cdots & \cdots \\ \vdots & \ddots & \vdots \\ \cdots & \cdots & \cdots \end{bmatrix} = \sum_{j=0}^{N} \mathbf{G}_j \qquad (31)$$

where the index $j=0$ corresponds to the main attractor of the system. The set of eigenvalues of the complete Jacobian are given by

$$\lambda^2 = \det(\mathbf{GI} - \lambda\mathbf{I}) = \det(\mathbf{G} - \lambda\mathbf{I}) \qquad (32)$$

with Λ being the eigenvalue with the maximum absolute value. In this case, only the contributions to the Jacobian given by each planet alone are considered:

$$\lambda_j^2 = \det(\mathbf{G}_j - \lambda\mathbf{I}), \quad j = 1, ..., N \qquad (33)$$

with λ_j^2 being the set of eigenvalues given by the contribution of j-th planet, and Λ_j the maximum eigenvalue of such set (it is clear that $\lambda^2 \neq \sum_j \lambda_j^2$). It can be found that

$$\Lambda_j = \frac{2\mu_j}{\|\mathbf{r} - \mathbf{r}_j\|^3} \qquad (34)$$

As a first criterion, the value of the eigenvalue contributions given by the single planets are compared with the one given by the main attractor (the Sun in the case of an interplanetary trajectory), with the fly-by event being identified when the ratio between the two reaches a given threshold, as shown in Fig. 1a. This definition of close approach is similar to the definition of SOI, as it considers the ratio between the accelerations of the approaching planet and the Sun. Fig. 1b also shows that the value of the eigenvalue defined in (34) presents a very high rate of variation during the fly-by, which starts increasing significantly earlier in time. For this reason, not only the value of the eigenvalue is considered, but also its time derivative, defined as

$$\dot{\Lambda}_j = 2\mu_j \frac{3(\mathbf{r} - \mathbf{r}_j)^T (\mathbf{v} - \mathbf{v}_j)}{\|\mathbf{r} - \mathbf{r}_j\|^5} \qquad (35)$$

A second criterion is thus defined, which also considers the ratio between the time derivatives of the eigenvalues of the single planets over the one of the main attractor. In this way, also the information of the approach speed is used in defining when a close approach occurs.

To summarise, two criteria have been considered to identify the fly-by condition during the integration:

$$\begin{aligned} \Lambda_j / \Lambda_0 &\geq \varepsilon_1 \\ \dot{\Lambda}_j / \dot{\Lambda}_0 &\geq \varepsilon_2 \end{aligned} \qquad (36)$$

These can be evaluated separately or combined.

Method	Order	Stages	Type	Time step	Property	Reference
RK	4 8	4 13	Explicit	Fixed step		Dormand and Prince, 1978 [23] Dormand and Prince, 1980 [24] Prince and Dormand, 1981 [25]
	5(4) 8(7)	7 13	Explicit	**Adaptive step**		
GLRK	4 6 8	2 3 4	**Implicit**	Fixed step	**Symplectic**	Jones et al., 2012 [16] Aristoff et al., 2012 [26] Butcher, 1964 [27]
RKN	6 8	6 26	Explicit	Fixed step	**Symplectic**	Calvo et al., 1993 [17] Dormand et al., 1987 [18]
SY	4 6 8	4 8 16	Explicit	Fixed step	**Symplectic, canonical**	Yoshida et al., 1990 [20] Neri, 1988 [28]

Table 1 - Selection of integration methods that were studied and implemented.

Eigenvalue contribution to Jacobian

a)

Eigenvalues time variations

b)
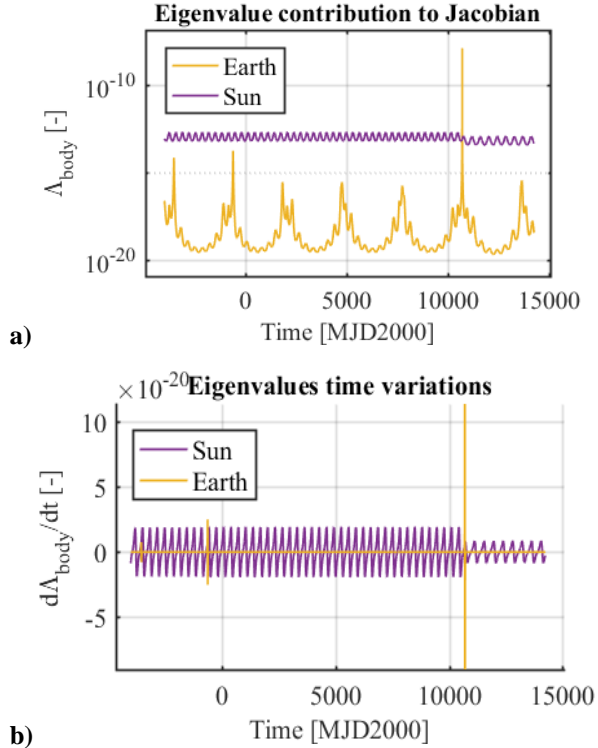
Fig. 1- Variation in time of the eigenvalues corresponding to the single contribution of the Earth and of the Sun during the propagation of Apophis from 1989 to 2039: a) values of the eigenvalues according to eq. (34); b) time variation of the eigenvalues according to eq. (35).

IV. RESULTS

IV.I. Application of LS

Three cases are considered to show a preliminary application of Line Sampling for the estimation of impact probability in a short time window: the launcher upper stage of Solo (which is analysed in detail in subsection IV.III), asteroid 2010 RF$_{12}$ and asteroid Apophis (which are treated in this subsection). These three examples were chosen purposely to show how LS performs when different levels of impact probability are expected.

2010 RF$_{12}$ is a small Near Earth Asteroid (NEA) that currently has the highest probability of hitting the Earth (around 6%) during a close fly-by in 2095; this event was chosen a test case due to the high expected impact probability, but the crossing of Low Earth Orbit (LEO,

considered under 2000 km from Earth's surface) was considered instead of a surface impact for computational reasons. The last case studies well-known asteroid Apophis, whose orbit may impact with Earth in 2036 depending on the uncertainty given by the observations in 2009; this event was chosen as a test case as more challenging for the application of LS, however the crossing of the geostationary (GEO) region was considered for computational reasons. In both cases, initial conditions were expressed in equinoctial parameters, with initial uncertainties in the form of diagonal covariance matrices, and then transformed into Cartesian coordinates for the propagation. These data were obtained by accessing the Near Earth Object Dynamic Site[1].

The comparison between the standard Monte Carlo method and LS is performed by analysing the following parameters: the number of initial random samples N_S (equal to the number of lines in the LS); the total number of orbital propagations N_P (larger than N_S for LS due to the iterative procedure that was used, and the preliminary propagations for the Markov Chain); the impact probability estimate $\hat{P}(I)$; the sample standard deviation $\hat{\sigma}$ of $\hat{P}(I)$; the coefficient of variation δ of the probability estimate, defined as the ratio of $\hat{\sigma}$ over $\hat{P}(I)$; the Figure of Merit (FOM) of the method, defined as $1/(\hat{\sigma}^2 \cdot N_p)$. The computational time was not considered due to the nature of the numerical integration and of the machine, and the number of simulations was preferred instead as reference parameter. The standard deviation and the coefficient of variation are used as indicators of the accuracy of the result, with lower values corresponding to lower variability of the result, while the FOM represents the efficiency of the method, with high desirable values [9].

---

[1]http://newton.dm.unipi.it/neodys

a)

b)
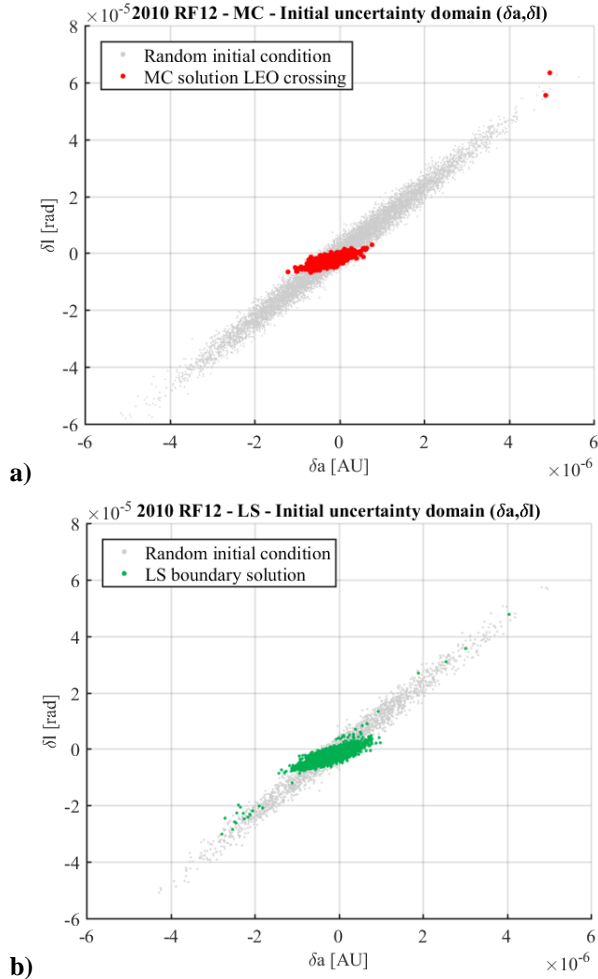
Fig. 2 - Visualisation of the initial dispersion in the uncertainty space $(\delta a, \delta l)$ in the case of asteroid 2010 RF$_{12}$: a) subdomain for LEO crossing found via standard MC, b) boudaries of the subdomain identified via LS.

	MCS	LS (σ^{MC})	LS (N_P^{MC})	LS (N_S^{MC})
N_S	1e4	1e3	1.6e3	1e4
N_P	1e4	~6e3	~1e4	~6e4
$\hat{P}(I)$	7.07e-2	7.29e-2	7.28e-2	7.23e-2
$\hat{\sigma}$	2.56e-3	1.13e-3	8.24e-4	2.79e-4
δ	2.76e1	1.56e-2	1.13e-2	3.87e-3
FOM	15.22	122.7	147.64	212.52

Table 2 - Application of Line Sampling to the case of asteroid 2010RF12 against the standard Monte Carlo Simulation.

Fig. 2 and Fig. 3 show the dispersions of the initial conditions obtained by random sampling from the given distributions in the three cases. In every plot, grey dots represent the initial conditions that don't lead to an impact with the considered body, red dots the starting conditions

that evolve in an impact identified through standard MC, while green dots represent the initial conditions at along the boundaries of the impact regions resulting from the LS application. In both figures, the dispersion is represented in terms of deviation of semi-major axis and equinoctial longitude from the nominal initial conditions.

All the propagations were carried out in dimensionless units (see ref. (12) paragraph III.I) using the adaptive Prince-Dormand RK8(7), with a relative tolerance of 10^{-12}.

Table 2 and Table 3 reports the results obtained in the cases of the asteroids with standard MC and LS, which in these cases was evaluated in three conditions, shown in the last three columns of the tables: in the first case a number the number of initial conditions was chosen in order to have comparable confidence levels (as values of $\hat{\sigma}$) between the two methods; in the second case the evaluation of the lines was stopped once the same number of orbital propagations N_P as the MC was reached; in the last case the same number of initial conditions and lines N_S was used across the two methods. The results show that, for both of the analysed examples, LS can be more efficient than the standard MC in estimating impact probability for the same confidence level (with fewer orbital propagations), and more accurate for the same number of initial samples (a lower value of variance), with generally lower values of δ and high values of the FOM, thanks to the analytical evaluations along each line (see expression (9)) which can compensate the use of extra evaluations employed by the LS in the iterative process. Moreover, by comparing the numerical results in the two tables one can observe that in the case of Apophis the FOM is much higher, confirming that LS becomes more convenient as the probability level decreases [9].

	MCS	LS (σ^{MC})	LS (N_P^{MC})	LS (N_S^{MC})
N_S	1e6	1e4	1e5	1.5e5*
N_P	1e6	~1e5	~1e6	~1.5e6
$\hat{P}(I)$	4.70e-5	5.38e-2	5.32e-5	5.33e-5
$\hat{\sigma}$	6.86e-6	1.18e-6	3.45e-7	2.87e-7
δ	6.85e0	2.18e-2	6.48e-3	5.39e-3
FOM	2.13e4	7.21e6	8.46e6	8.13e6

Table 3 - Application of Line Sampling to the case of asteroid Apophis against the standard Monte Carlo Simulation.

IAC-17-C1.9.5
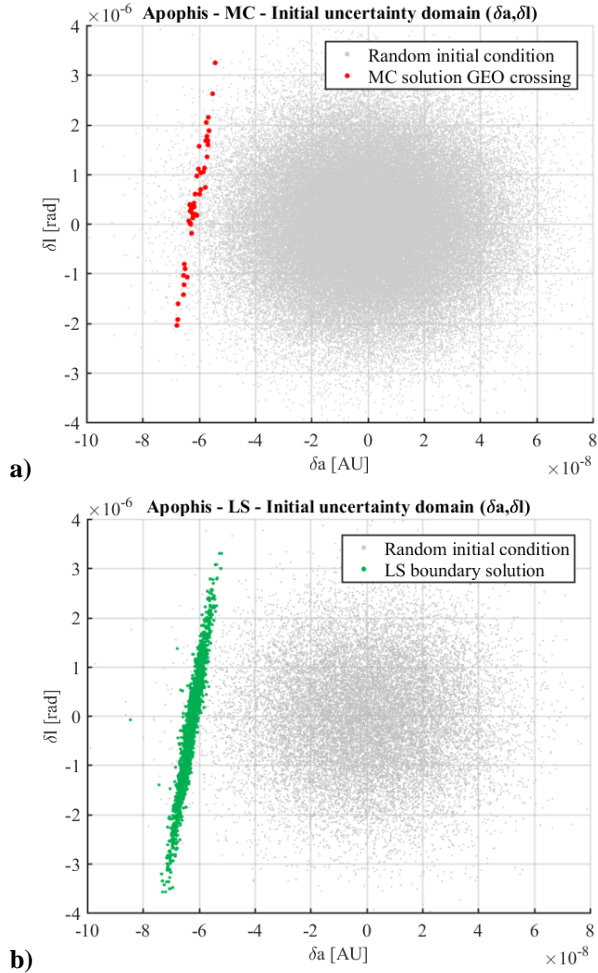
Fig. 3 - Visualisation of the initial dispersion in the uncertainty space $(\delta a, \delta l)$ in the case of asteroid Apophis: a) subdomain for GEO crossing found via standard MC, b) boundaries of the subdomain identified via LS.
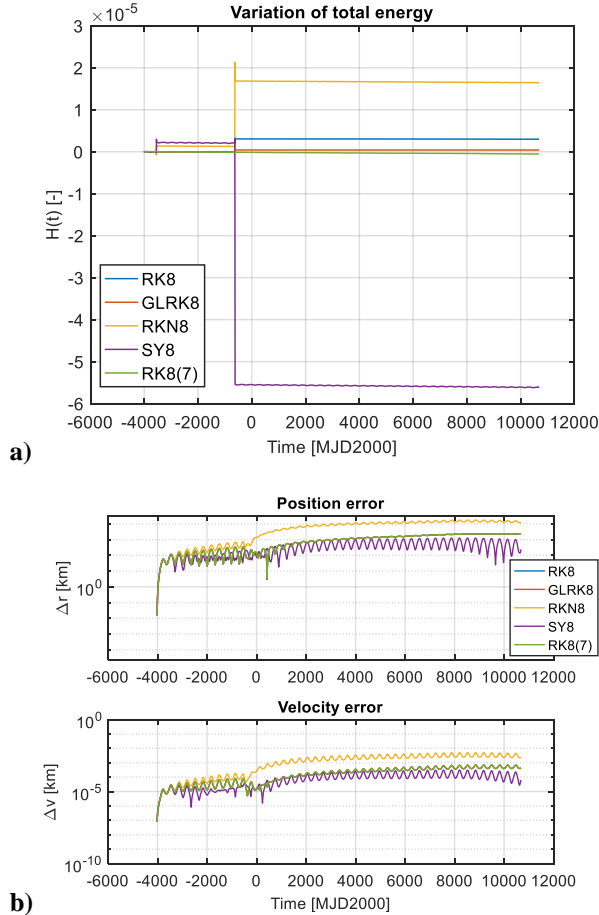
IV.II. Comparison of different integration methods

A series of tests were carried out to show how the considered symplectic and non-symplectic 8th order methods perform for the integration of the n-body equations of motion expressed in Eq. (13). The case in exam is the propagation of asteroid Apophis between 1989 and 2039, with the ephemerides for every planet obtained from the JPL SPICE model. Following the option already available in SNAPPshot [4], the initial step was determined for all the fixed-step and regularised step methods via a single-step run of RK8(7) using a relative tolerance of 10^{-12}. The value of the Hamiltonian function shown in Fig. 4 to Fig. 6 is the one introduced in Eq. (15): the expected value is thus analytically zero during the whole propagation, with variations only due to numerical errors.

Different cases are shown, to differentiate between regular and non-regular dynamics (the latter one represented by a fly-by during the propagation).
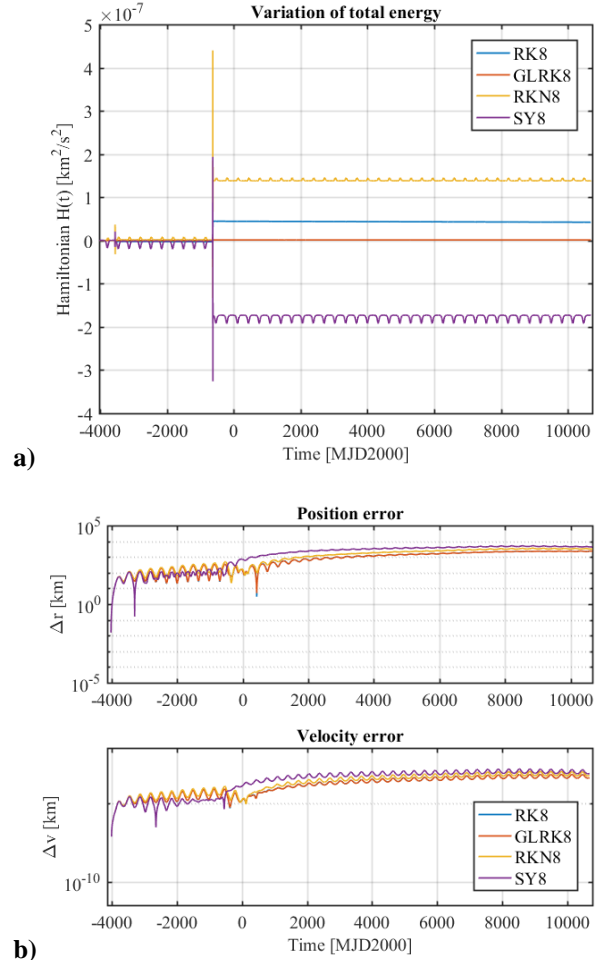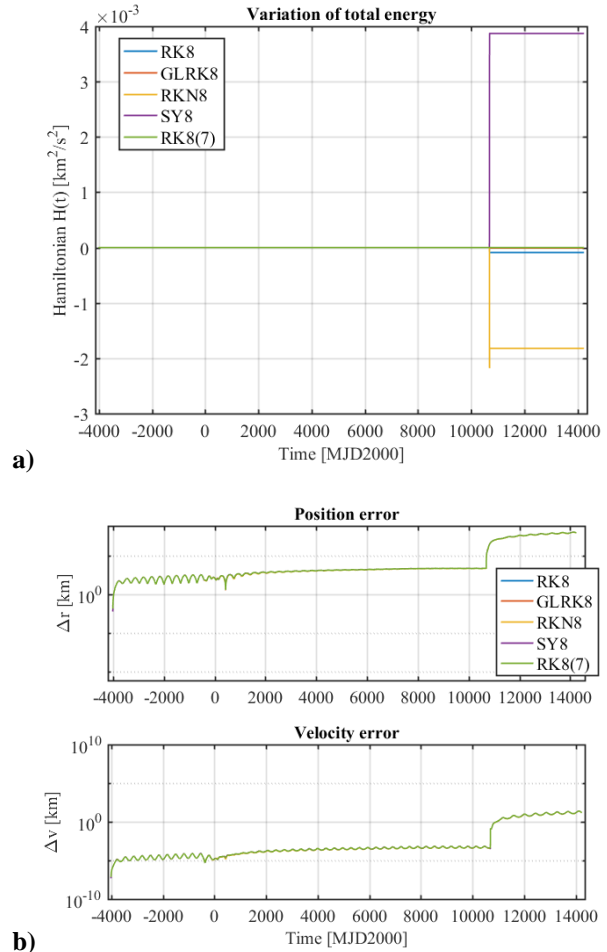

Fig. 4 - Comparison among the different fixed-step integration methods for the propagation of asteroid Apophis from 1989 to 2029, a) Value of the Hamiltonian function in time, b) position and velocity errors in time with respect to the reference ephemerides.

Fig. 4a shows the value of the Hamiltonian function for the propagation of Apophis from 1989 to 2029 (before the predicted fly-by with Earth) using a fixed step size. One can observe that, when the dynamics is regular, the symplectic methods (GLRK, RKN and SY, respectively the red, yellow and purple lines) preserve the value of the Hamiltonian as expected, with bounded oscillations but no secular drift, while the non-symplectic RK method (blue line) shows a small linear variation; in Fig. 4b, the implicit RK method shows a comparable level of error over the state (position and velocity) of Apophis as the non-symplectic RK method.

a)

b)

Fig. 5 - Comparison among the different regularised-step integration methods for the propagation of asteroid Apophis from 1989 to 2029, a) Value of the Hamiltonian function in time, b) position and velocity errors in time with respect to the reference ephemerides.

The same time interval was considered in the propagation shown in Fig. 5, with the use in this case of step regularisation for all the integration schemes. Here also the non-symplectic adaptive method RK8(7) was used as a reference. In this case, as expected, the value of the Hamiltonian shows a secular drift also for symplectic methods due to the variation of the timestep. The Yoshida method (SY), however, shows a better behaviour in terms of error over the state.


a)

b)

Fig. 6 - Comparison among the different regularised-step integration methods for the propagation of asteroid Apophis from 1989 to 2039, a) Value of the Hamiltonian function in time, b) position and velocity errors in time with respect to the reference ephemerides.

The long-term behaviour seen in Fig. 4 and Fig. 5, however, changes when a flyby occurs during the propagation. Fig. 6 also shows the propagation of Apophis, in this case in the window 1989-2039 in order to include also the 2029 fly-by with Earth. The increase of non-linearity of the dynamics during the fly-by can be visualised in the jump of several orders of magnitude that the total energy and the state error undergo at the epoch of the flyby, affecting in similar ways all the integration schemes and hiding the approximation errors of the integrations. Similar jumps can also be observed in Fig. 4 and Fig. 5, again due to close approaches with Earth. In these cases, however, the variation in the total energy is much more contained than in the case of a deep fly-by, due to the larger distance from the planet.

Fig. 7 shows the performance of the integration methods both in terms of accuracy and in terms of efficiency: the maximum errors (energy, position and velocity) are related to the computational time to perform one integration step; the energy error is defined in terms of maximum value of the Hamiltonian function (that is, deviation from the zero initial value) as

$$\Delta H_{max} = \max \left| H(t) - H_0 \right| = \max \left| H(t) \right|,$$ while the position

and velocity errors are defined as maximum deviation from the JPL SPICE ephemerids used as reference. From the results presented here it can be observed that the symplectic implicit Runge-Kutta (GLRK) and the Yoshida method (SY) are the most accurate in terms of position error in time among the ones taken into exam, respectively with a fixed-step and a regularised step. However, the GLRK in both cases shows a better conservation of energy in time, also when close approaches are present. The higher computational time with respect to the other integration methods is due to the fixed-point iterations to solve the implicit problem at every step. For this reason, a focus on better methods to solve implicit systems of non-linear equations could improve the efficiency of the integrator.
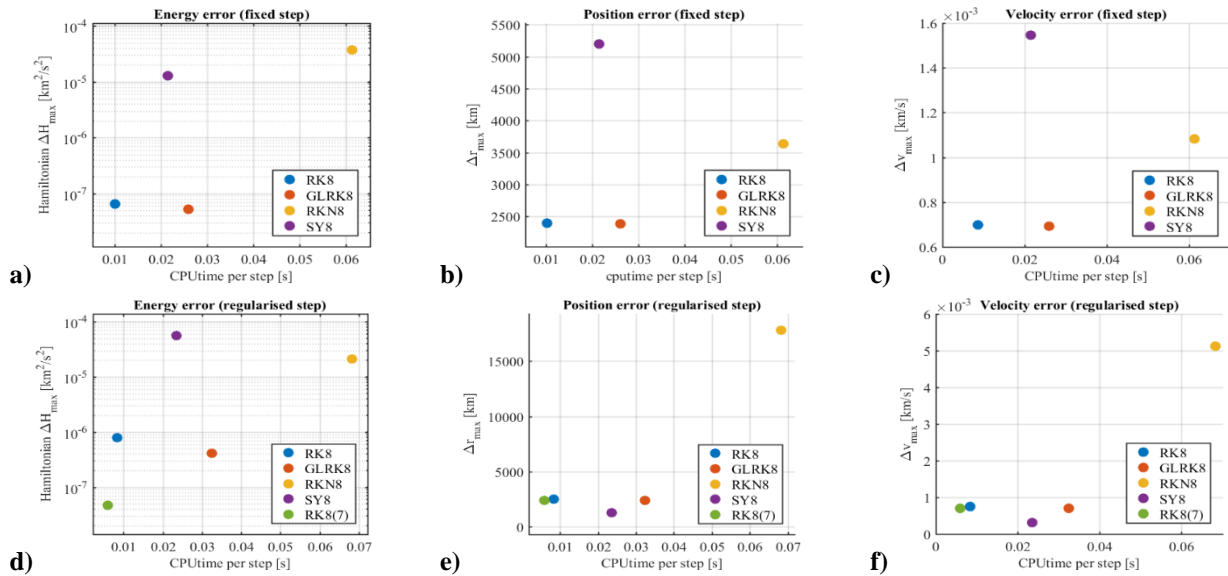

Fig. 7 – Plots showing the efficiency and the accuracy of the methods in terms of computational time per step (x axes) and maximum error (y axes): a) and d) show the maximum energy error; b) and e) the maximum position error; c) and f) the maximum velocity error; the top three plots refer to fixed-step propagations, the bottom ones to propagation with step regularisation.

IV.III. Mission case: Launcher upper stage of Solo

Solo (Solar Orbiter) is a planned Sun-observing satellite, under development by ESA. The case under study refers to the launch option in October 2018, presenting a fly-by of Venus during the first year after leaving Earth's orbit [29]. In this case, the planetary protection analysis is focused on the Atlas V upper stage, as it also follows a trajectory that will bring it close to Venus. Although this planet has no explicit planetary protection requirements, the Venus fly-by represents an interesting case to test the new technique. Initial data are taken from [4], with initial conditions and covariance matrix expressed in Cartesian coordinates.

	MC	LS (σ^{MC})
N_S	54114	~54000
N_P	54114	~250000
$\hat{P}(I)$	4.20e-2	4.28e-2
$\hat{\sigma}$	8.60e-4	5.40e-4
Δ	2.06e-2	1.26e-2
FOM	25.06	13.45

Table 4 - Results of the application of the LS for the launcher of Solo during its first fly-by of Venus, against the standard Monte Carlo method; LS was evaluated in order to obtain a confidence level comparable with MC.
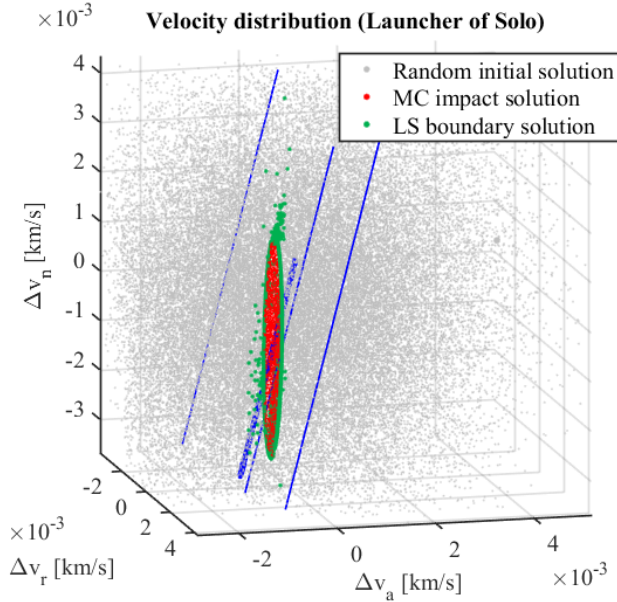
Fig. 8 - Impact region inside the initial velocity dispersion for the launcher of Solo spacecraft: the initial conditions leading to an impact with Venus are shown in red, while in green are shown the borders of the impact region as found by the Line Sampling. Blue lines represent the reference direction α (thick line) and the sampling lines (thin lines).

Fig. 8 shows the dispersion of the MC runs in terms of the deviation from the initial nominal velocity: Δv_r, the deviation in the radial direction, Δv_a, the deviation in the along-track direction, and Δv_n, the deviation in the direction normal to the instantaneous orbital plane, for the relative velocity with respect to the Earth. The colours in the plots have the same meaning of the plots for the asteroids.

In the case of Solo, while the LS can well identify the boundary of the impact subdomain (see Fig. 8), the results in **Error! Reference source not found.** show that the method can only obtain a comparable level of accuracy with a comparable number of initial samples, which results in a higher number of propagations and thus computational time. The visible difference between the performance of the LS in the case of Solo and of the asteroids is caused by two main reasons: the high value of the impact probability, which makes the method less efficient in terms of number of initial random samples that have to be generated and propagated; the shape and size of the impact region, which is distributed across the uncertainty domain in the case of Apophis and 2010 RF$_{12}$, with almost every line crossing it during the sampling, while confined in the case of Solo,

causing many lines to miss it, reducing the efficiency of the method with a waste of orbital propagations. This phenomenon can be seen in Fig. 8, where some of the blue lines used for the sampling do not intersect the impact region. Another factor that affects the performance of the LS method is the accuracy of the iterative process that identifies the intersections of the lines with the impact subdomain.

V. CONCLUSIONS

This paper presented a plan to improve the verification of compliance to planetary protection requirements for interplanetary missions, by introducing alternative numerical techniques to obtain a higher accuracy in the orbital propagation and a higher efficiency in the sampling of the initial conditions. Two main strategies were introduced: the Line Sampling method proved to be more competitive than the standard Monte Carlo sampling in the estimation of impact probability by requiring a lower computational effort to reach similar confidence levels, especially in cases where the expected probability is very low; symplectic methods demonstrated that the solution of the integration can be made closer to the actual physical behaviour of the dynamics, by preserving the total energy of the system on the long term, although numerical issues are encountered when the orbital propagation includes close fly-by with celestial bodies.

The final goal of the work presented here will be the combined application of the two strategies introduced in this paper (on the numerical integration side, and on the sampling side) in order to improve the available tools for planetary protection analysis. This will require to solve the current limitations of the two approaches and to improve each of them and make them more effective.

On the integration side, the analysis of the already available symplectic and non-symplectic methods will continue, alongside an examination of alternative formulations of the dynamics.

On the side of uncertainty sampling, we aim at improving the identification of the roots of the objective functions along the lines, and to improve the general efficiency of the Line Sampling, in particular by devising an analytical expression of the confidence interval given by this method, allowing to identify the minimum number of initial samples (lines) necessary to reach a given confidence level.

ACKNOWLEDGMENTS

VI. REFERENCES

[1] Kminek G., *ESA planetary protection requirements*, Technical Report ESSB-ST-U-001, European Space Agency, February 2012.

[2] Jehn R., *Estimation of impact probabilities of interplanetary Ariane upper stages*, in 30th International Symposium on Space Technology and Science, Jul. 2015.

[3] Wallace M.S., *A massively parallel bayesian approach to planetary protection trajectory analysis and design*, in AAS/AIAA Astrodynamics Specialist Conference, Aug. 2015.

[4] Colombo C., Letizia F., Van den Eynde J., Jehn R., *SNAPPshot, ESA planetary protection compliance verification software. Final report*, ESA 2016, ESA ref. ESA-IPL-POM-MB-LE-2015-315.

[5] Letizia F., Colombo C., Van den Eynde J., Armellin R., Jehn R., *SNAPPSHOT: Suite for the numerical analysis of planetary protection*, 6th International Conference on Astrodynamics Tools and Techniques (ICATT), 14-17 Mar. 2016, Darmstadt.

[6] Letizia F., Colombo C., Van den Eynde J., Jehn R, *B-plane visualisation tool for uncertainty evaluation*, The 26th AAS/AIAA Space Flight Mechanics Meeting, Napa, CA, 14-18 Feb. 2016, AAS 16-438.

[7] Hairer, E., Lubich, C., Wanner, G.: *Geometric Numerical Integration*, 2nd edn.. Springer Series in Computational Mathematics, vol. 31. Springer, Berlin (2006).

[8] Zio E., *The Monte Carlo Simulation Method for System Reliability and Risk Analysis*, 1st edn., Springer Series in Reliability Engineering, Springer-Verlag London (2013).

[9] Zio E., Pedroni N., *Subset Simulation and Line Sampling for Advanced Monte Carlo Reliability Analysis*, Proceedings of the European Safety and RELiability (ESREL) 2009 Conference, 2009, pp.687-694.

[10] Romano M., Losacco M., Colombo C., Di Lizia P., *Estimation of impact probability of asteroids and space debris through Monte Carlo Line Sampling and Subset Simulation*, KePASSA Workshop 2017.

[11] Rosenblatt M., *Remarks on a Multivariate Transformation*, Ann. Math. Statist. 23 (1952), no. 3, 470--472. doi:10.1214/aoms/1177729394. http://projecteuclid.org/euclid.aoms/1177729394.

[12] Morbidelli A., *Modern Celestial Mechanics, Aspects of Solar System Dynamics*, London: Taylor & Francis, 2002, ISBN 0415279399.

[13] Sanz-Serna J.M., *Symplectic Runge-Kutta and related methods: recent results*, Physica D Volume 60 Issue 1-4, Nov. 1, 1992, Pages 293-302.

[14] Quarteroni A., Sacco R., Saleri F., *Numerical Mathematics*, Texts in Applied Mathematics, Springer Berlin Heidelberg, 2010, ISBN 9783540498094.

[15] Rangarajan G., *Symplectic integration of nonlinear Hamiltonian systems*, J Phys (1997) 48: 129, https://doi.org/10.1007/BF02845627.

[16] Jones, B. A. and R. L. Anderson, *A Survey of Symplectic and Collocation Integration Methods for Orbit Propagation*, 22nd Annual AAS/AIAA Space Flight Mechanics Meeting, Charleston, SC, January 29 - February 2, 2012.

[17] Calvo M., Sanz-Serna J., *High-Order Symplectic Runge–Kutta–Nyström Methods*, SIAM J. SCI. COMPUT., Vol. 14, No. 5, pp. 1237-1252, September 1993.

[18] Dormand J., El-Mikkawy M., Prince P., *Families of Runge-Kutta-Nystrom Formulae*, Journal of Numerical Analysis (1987) 7, 235-250.

[19] Forest E., Ruth R.D., *Fourth-order symplectic integration*, Physica D: Nonlinear Phenomena 43.1 (1990): 105-117.

[20] Yoshida H., *Construction of higher order symplectic integrators*, Physics Letters A 150(5-7):262-268, November 1990.

[21] Debatin F., Tilgner A., Hechler F., *Fast numerical integration of interplanetary orbits*, In Second International Symposium on Spacecraft Flight Dynamics, 1986.

[22] Amato D., Baù G., Bombardelli C., *Accurate orbit propagation in the presence of planetary close encounters*, Monthly Notices of the Royal Astronomical Society, Volume 470, Issue 2, 11 September 2017, Pages 2079–2099.

[23] Dormand J. and Prince P., *New Runge-Kutta algorithms for numerical simulation in dynamical astronomy*, Celestial Mechanics, 18(3):223–232, 1978.

[24] Dormand J. and Prince P., *A family of embedded Runge-Kutta formulae*, Journal of Computational and Applied Mathematics, 6(1):19–26, 1980. ISSN 03770427.

[25] Prince P. and Dormand J., *High order embedded Runge-Kutta formulae*, Journal of Computational and Applied Mathematics, 7(1):67–75, 1981. ISSN 03770427.

[26] Aristoff, J.M., Poore, A.B, *Implicit Runge–Kutta methods for orbit propagation*, Proceedings of the AIAA/AAS Astrodynamics Specialist Conference, Minneapolis, MN, August. Paper AIAA 2012–4880 (2012).

[27] Butcher J., *Implicit Runge-Kutta processes*, Math. Comp. 18 (1964), 50-64.

[28] Neri F., *Lie algebras and canonical integration*, Department of Physics, University of Maryland, reprint (1988).

[29] European Space Agency, *Solar Orbiter, Exploring the Sun-heliosphere connection*, Definition Study Report, ESA/SRE(2014)11, July 2011.